SUPPLEMENTARY DATA

Supplementary Figure 1. Generation of kallistatin-TG mice. A, Diagram of the human kallistatin transgene construct. B and C, Kallistatin levels in the serum (B) and retina (C) of the WT and kallistatin-TG mice. D, Mouse kallistatin levels in the retina of the WT and kallistatin-TG mice. The retinas were isolated after perfusion, and homogenized for kallistatin ELISA (R&D) analysis, normalized by total protein concentrations in the retina. All values are mean ± SD. n=10. ***P<0.001,*P<0.05.

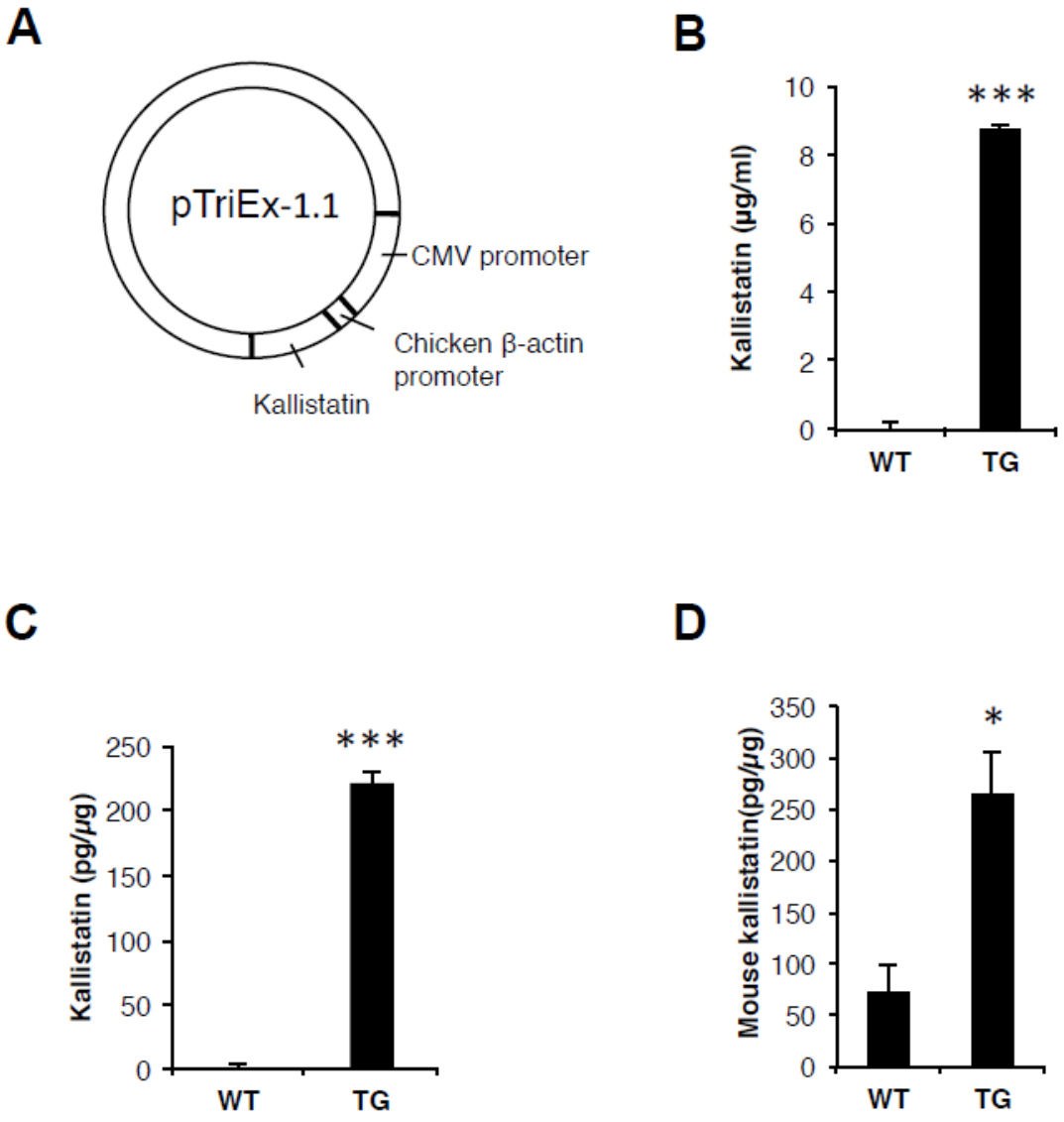

SUPPLEMENTARY DATA

Supplementary Figure 2. The kallistatin-TG mice display no overt behavioral or developmental abnormalities. A, H&E-stained eye sections from 4-month-old WT and kallistatin-TG mice. The images are representatives from 5 mice of each type. GCL, ganglion cell layer; INL, inner nuclear layer; ONL, outer nuclear layer; RPE, retinal pigment epithelium. Scale bar: 50 μm. B, Quantification of thickness of the retina of WT and kallistatin-TG mice at 4 months of age. n=6. C, ERG amplitudes of WT and kallistatin-TG mice at 4 months of age. Dark-adapted (scotopic/rod-associated) and light-adapted (photopic/cone-associated) ERGs were recorded from WT and kallistatin-TG mice, and the amplitudes of the A and B waves compared. All values are mean ± SD. n=10.

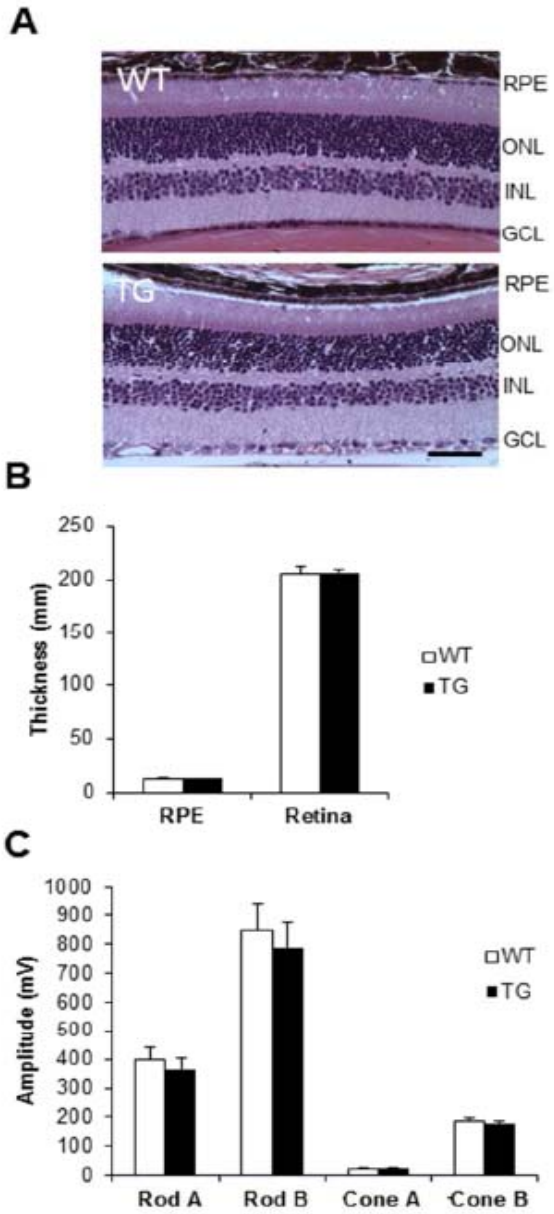

SUPPLEMENTARY DATA

Supplementary Figure 3. Kallistatin down-regulates ICAM-1 expression in HRCEC. A, HRCEC were exposed to WCM with different concentrations of purified kallistatin for 24 hr, with LCM as control. Total protein concentrations in each well were brought to the same by the addition of BSA. B, ICAM-1 levels were semi-quantified by densitometry, normalized by β-actin levels and expressed as % of the LCM control. All values are mean ± SD. n=3. **P*<0.05.

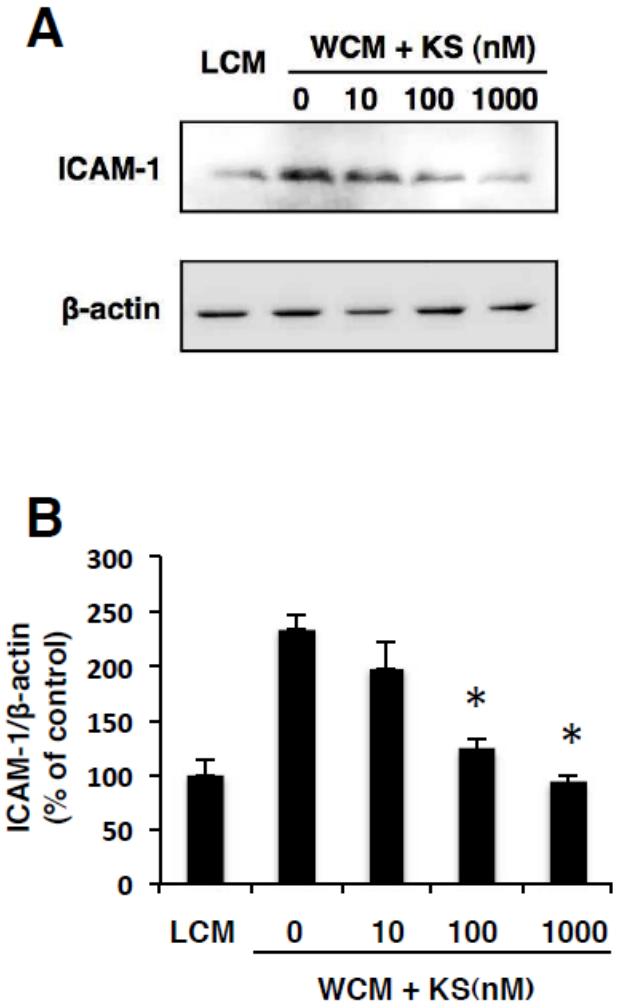

SUPPLEMENTARY DATA

Supplementary Figure 4. $CD11b^+$ leukocytes are significantly elevated in the retinas of Akita mice and reduced in Akita×kallistatin-TG mice. The mice were thoroughly perfused with saline to remove circulating leukocytes from the blood vessels. The retinas were then dissected and single cell suspension generated. The retinal cells were separately stained with antibodies for CD11b, Gr-1, CD3 and CD19, and analyzed with flow cytometry. A, $CD11b^+$ cells from the retinas of WT, Akita, and Akita×kallistatin-TG mice. B, Quantification of $CD11b^+$ cells. C, $Gr\text{-}1^+$ cells from the retinas of WT, Akita, and Akita×kallistatin-TG mice. D, Quantification of $Gr\text{-}1^+$ cells. E, $CD19^+$ cells from the retinas of WT, Akita, and Akita×kallistatin-TG mice. F, Quantification of $CD19^+$ cells. G, $CD3^+$ cells from the retinas of WT, Akita, and Akita×kallistatin-TG mice. H, Quantification of $CD3^+$ cells. All values are mean ± SD. n=8. **P*<0.05, ***P*<0.01.

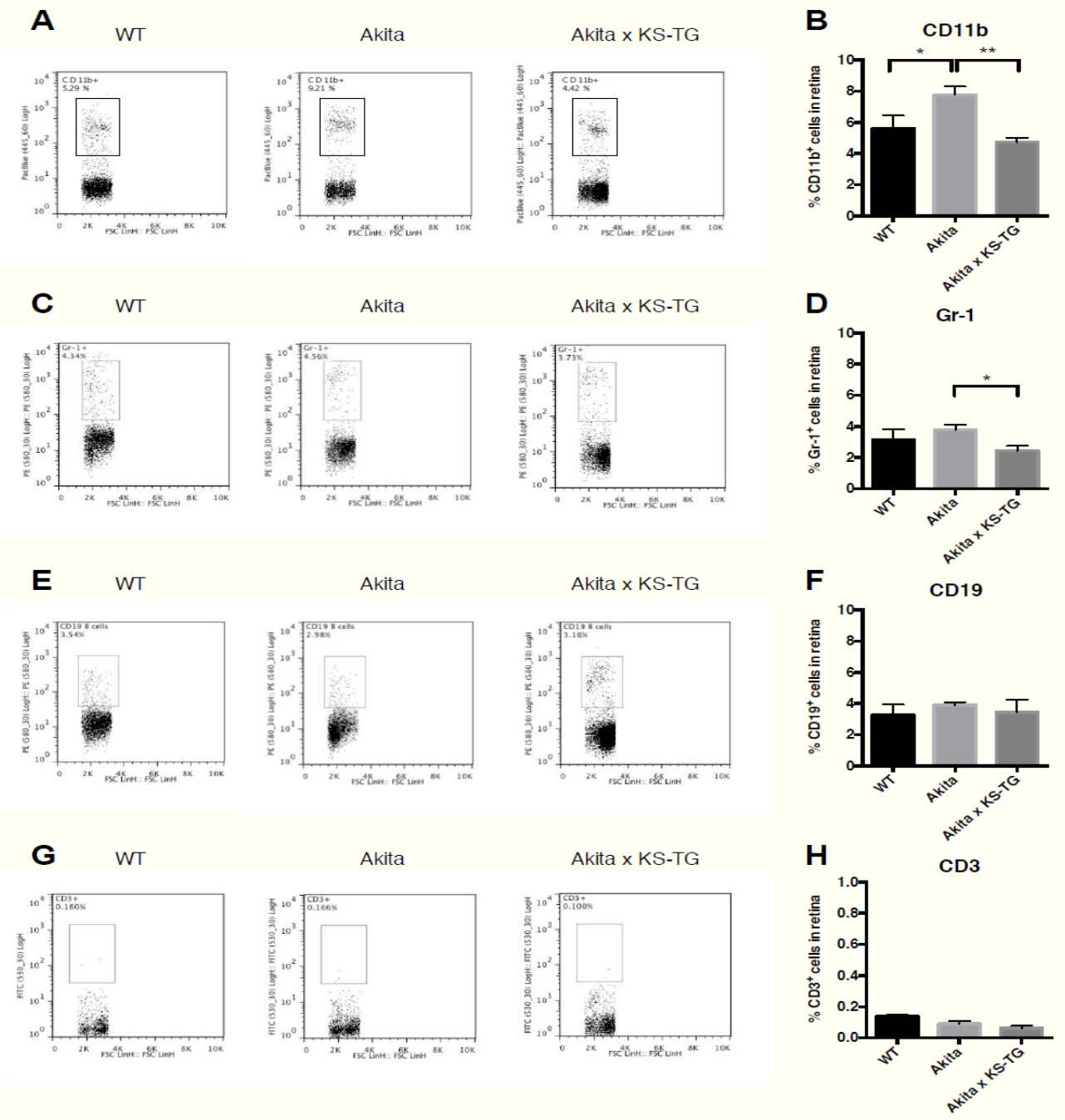

SUPPLEMENTARY DATA

Supplementary Figure 5. Kallistatin inhibits TOPFLASH activity induced by Wnt3a in HMCs and HRCECs. A and B, Both HMCs (A) and HRCECs (B) were infected with lentivirus to deliver the TCF/LEF-responsive elements and renilla vectors. The cells were exposed to LCM or WCM for 24 hr, and incubated with different concentrations of purified kallistatin protein. TOPFLASH activities was measured using the luciferase assay. All values are mean ± SD. n=6. **P*<0.05, **P<0.01.

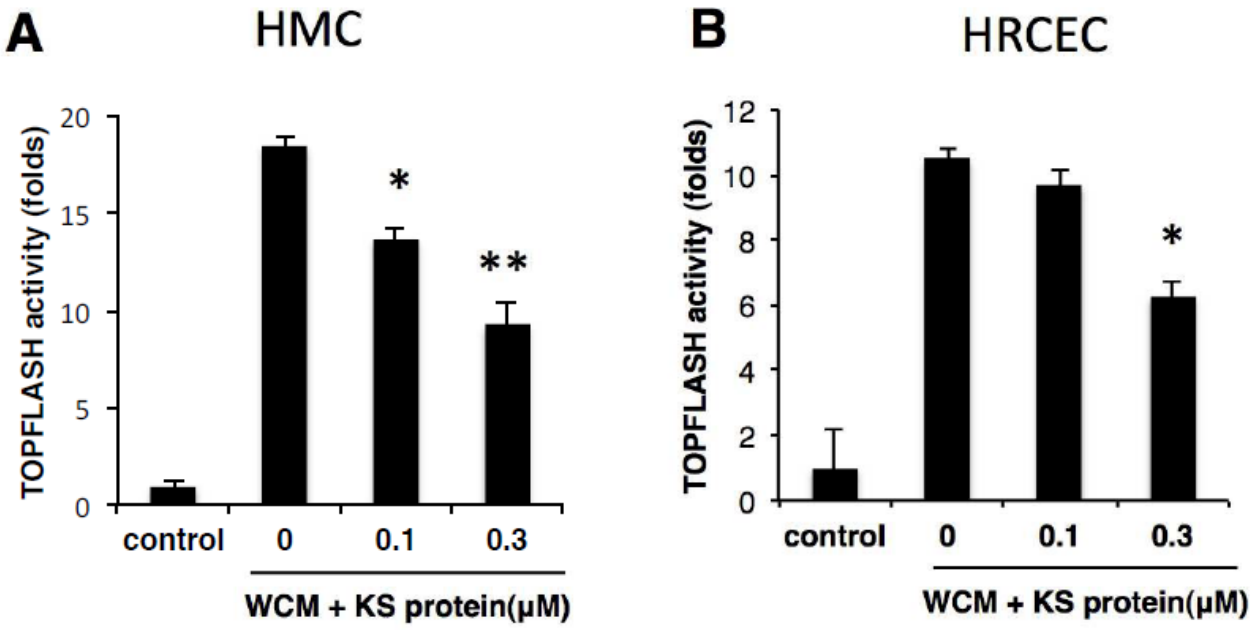

SUPPLEMENTARY DATA

Supplementary Figure 6. Kallistatin does not inhibit Wnt signaling induced by LiCl. A, hTERT-RPE-1 cells were transfected with the TOPFLASH vector and 0, 0.1 and 0.3 μg of the kallistatin expression vector. Total DNA concentrations were brought to the same by supplementing with an empty vector. At 24 hr following the transfection, the cells were exposed to 10 mM LiCl with or 10 mM NaCl (as control) for another 24 hr. TOPFLASH activity was measured using luciferase assay. B, hTERT-RPE-1 cells were transfected with the TOPFLASH vector. The cells were exposed to 10 mM LiCl, with NaCl as control, and 0.6 μM of purified kallistatin protein for 24 hr. TOPFLASH activity was measured using luciferase assay (mean ± SD, n=6). N.S, not significant.

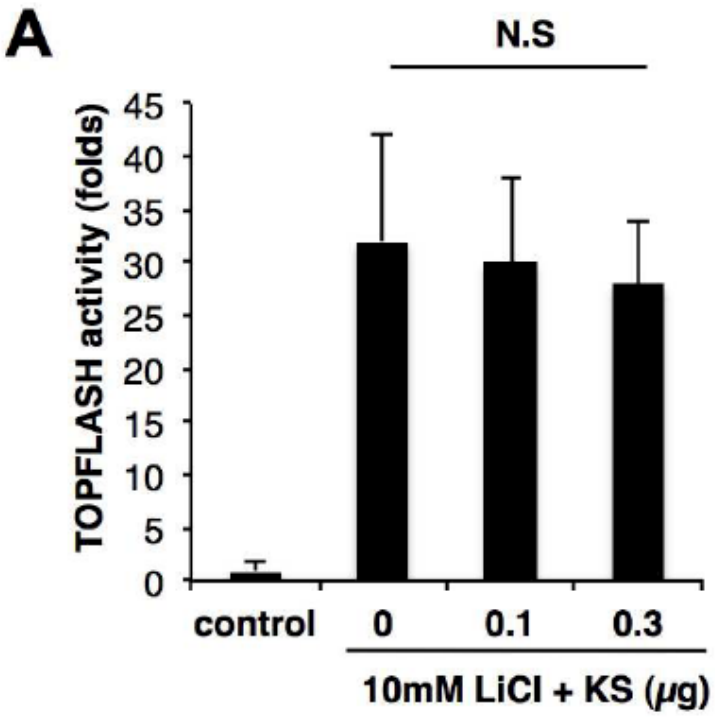

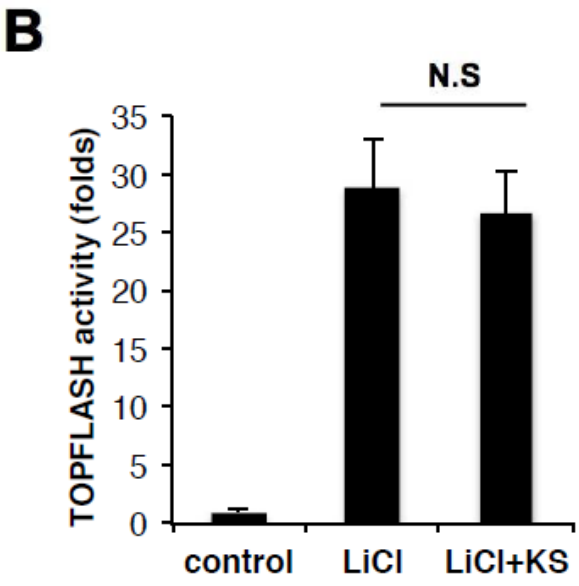

SUPPLEMENTARY DATA

Supplementary Figure 7. Coomassie blue staining for purified kallistatin protein. 5pg purified protein was loaded in the SDS-PAGE gel and stained with 0.1% Coomassie stain solution.

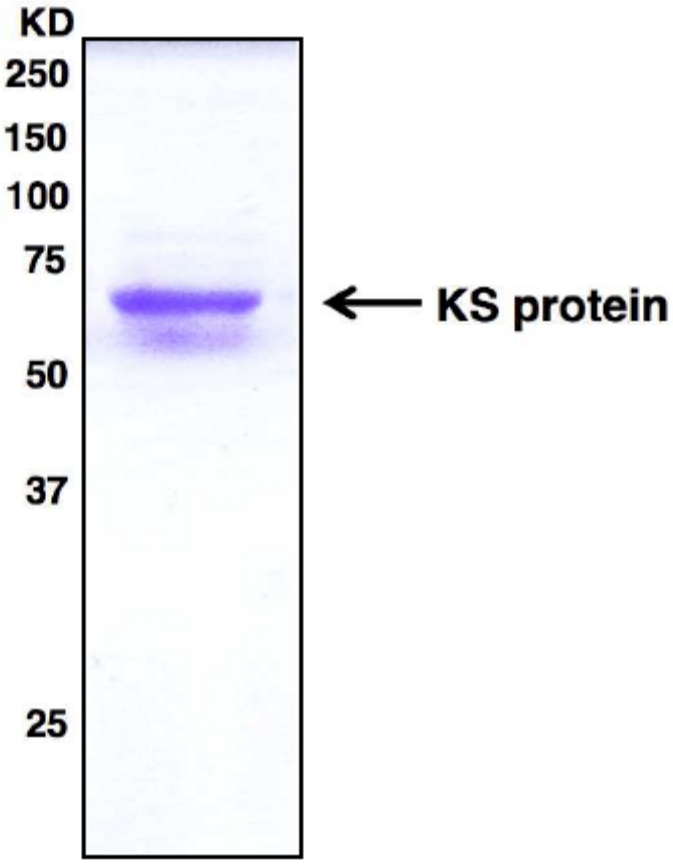

SUPPLEMENTARY DATA

Supplementary Figure 8. Negative control for co-immunoprecipitation of kallistatin. Immunoprecipitation was performed with the Ni-NTA resin in LRP6N-Myc conditioned medium with or without recombinant cellular retinol-binding protein with HIS-tag (CRBP-HIS) protein. Precipitates and input samples were immunoblotted with antibodies for Myc-tag and His-tag to identify LRP6N-Myc and CRBP-HIS proteins.

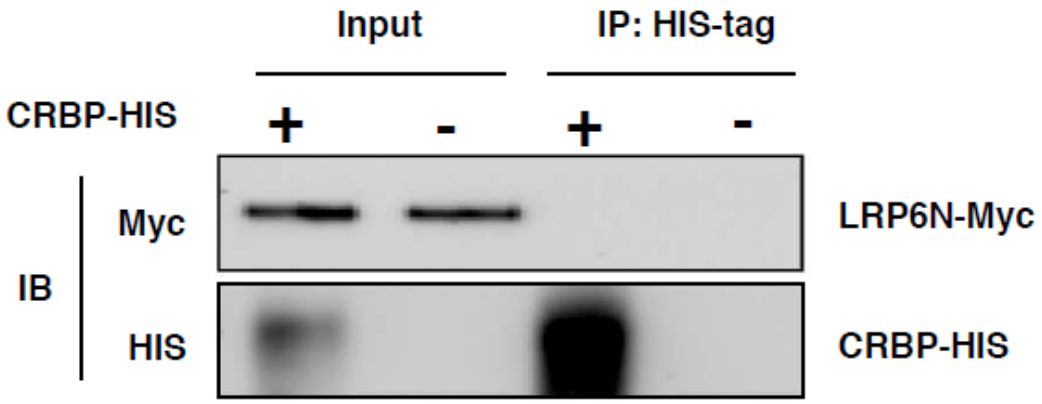

Supplementary Figure 9. Retinal vasculature of transgenic mice under normal conditions. A, The vasculature of retinal flat mounts was visualized after injection of FITC-dextran into adult WT mice and kallistatin-TG mice. Scale bar: 50 μm. B, Quantification of vessel branching of the retinas of WT and kallistatin-TG mice (mean ± SD, n=5). N.S, not significant.

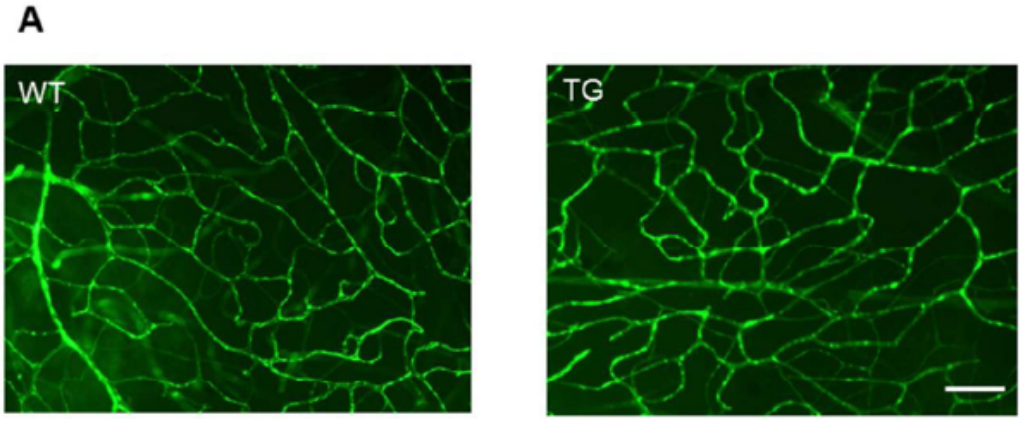

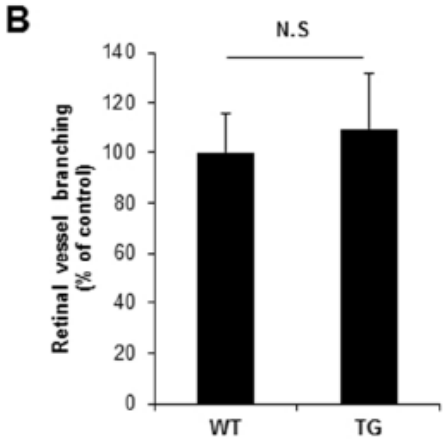

SUPPLEMENTARY DATA

Supplementary Figure 10. Wnt3a competes with Kallistatin binding to LRP6N. ELISA plates were coated with conditioned medium of LRP6N overnight. Purified kallistatin (25 nM) was mixed with different concentrations of purified Wnt3a protein and incubated in the wells. The signals were developed using a Biotin-labeled secondary antibody for kallistatin and measured by absorbance at 450 nm using a microplate reader.